Research Square

Preprints are preliminary reports that have not undergone peer review.
They should not be considered conclusive, used to inform clinical practice,
or referenced by the media as validated information.

An oxidative stress response gene model for the prediction of prognosis and therapeutic responses in hepatocellular carcinoma

Xiujun Cai (caixiujunzju@163.com)
Sir Run Run Shaw Hospital

Junjie Hong
Sir Run Run Shaw Hospital

Research Article

Keywords: hepatocellular carcinoma, oxidative stress, gene signature, prognosis, chemotherapy, immunotherapy

Posted Date: March 8th, 2022

DOI: https://doi.org/10.21203/rs.3.rs-1142038/v2

License: This work is licensed under a Creative Commons Attribution 4.0 International License.
Read Full License

Abstract

Background:

Oxidative stress response genes are critical for the development and progression of hepatocellular carcinoma (HCC). Still, the predictive value for prognosis and treatment response of oxidative stress response genes needs further elucidation.

Results:

We obtained the transcriptomic data and corresponding clinicopathological information of HCC patients from The Cancer Genome Atlas (TCGA) and International Cancer Genome Consortium (ICGC) databases. Oxidative stress response genes (OSRGs) were retrieved from the MSigDB database. LASSO Cox regression analysis was utilized to establish an integrated multi-gene signature in the TCGA cohort, and its prediction performance was validated in the ICGC cohort. The risk score of each patient ware determined by the multi-gene signature. The CIBERSORT algorithm was employed to evaluate the immune cell infiltration. Response rate to immune checkpoint inhibition (ICI) therapy was assessed using a TIDE platform. Tumor mutation burden was estimated using VarScan processed somatic mutation data. The drug activity data from the Cancer Genome Project and NCI-60 human cancer cell lines were used to predict sensitivity to chemotherapy. Finally the established gene signature comprises *G6PD, MT3, CBX2, CDKN2B, CCNA2, MAPT, EZH2, and SLC7A11*. Patients with high risk scores had shorter overall survival. The risk score was identified as an independent prognostic marker. The immune cell infiltration patterns, response rates to immune checkpoint inhibition (ICI) therapy, and the estimated sensitivity of 89 chemotherapeutic drugs were associated with risk scores. Individual prognostic gene was also associated with the susceptibility of various FDA-approved drugs.

Conclusion:

Our study indicates that an integrated transcriptomic analysis may provide a reliable molecular model that better predicts diagnosis and forecasts the response of ICI therapy and chemotherapy.

Introduction

Hepatocellular carcinoma (HCC) ranks fifth among all malignancies worldwide and is the second common cause of cancer-associated deaths [1]. Despite advances in therapeutic measures, the prognosis of HCC has improved very little over the last two decades. In clinical practice, prognosis prediction and treatment recommendation highly depend on clinical characteristics and pathological features, whose efficacy of prophecy is usually unsatisfactory because of HCC's high heterogeneity. Hence, novel prognostic markers that can better inform treatment strategies and adequately predict the prognosis are urgently needed. The recent technological progress in microarray technology has permitted that integrating multiple prognosis-related genes into a single prognostic model became a powerful approach to improve the accuracy of prediction.

It is well known that cancer cells are generally under stressful biological conditions, among which oxidative stress is one the most representative [2]. Increased oxidative stress is a hallmark of the cancer microenvironment, reflected by the elevated intracellular levels of reactive oxygen species (ROS) [3, 4]. ROS are highly reactive oxygen chemicals, constituting peroxides, superoxide, hydroxyl radicals, and hydrogen peroxide. Dysregulated ROS in cancer cells may be attributed to the activation of the oncogene, hypoxia, and extracellular stimuli, such as chemotherapy and radiotherapy[5-7]. Excessive generation of ROS can be lethal to cancer cells, as it induces cell apoptotic death via DNA repair disorders, proteins damage, and lipid peroxidation [8]. Cancer cells exploit endogenous adaption, including transcriptomic and proteomic modulation, to survive under pressure from oxidative stress. Earlier studies reported that multiple genes, known as oxidative stress response genes (OSRGs), are involved in the endogenous adaption of cancer cells. For instance, the proteins encoded by *MGST1/3, G6PD, GSR, and GPX2/4* play vital roles in glutathione synthesis, which serves as an antioxidant defender in cancer cells[9]. Besides, *TXN*, together with *PRDXs*, reduces intracellular hydrogen peroxide and oxidized proteins[10]. Generally, these genes are upregulated in tumor tissues and indicate poor prognoses, making them promising therapeutic targets.

Although OSRGs are essential for the proliferation, progression, and migration of HCC cells[4], the prognosis prediction and therapy recommendation value of OSRGs has not been well elucidated. In the present study, we conducted a transcriptomic analysis using HCC gene expression profiling data from The Cancer Genome Atlas (TCGA) and the International Cancer Genome Consortium (ICGC) databases. First, in TCGA cohort, the OSRGs related to the overall survival (OS) were filtered out, then an eight-gene prognostic signature was established, and its robustness was evaluated with the ICGC cohort. We also analyzed the correlation between the tumor-infiltrating immune cells and prognostic risk scores. In addition, immune checkpoints expression, immune checkpoint inhibition (ICI) therapy response rate, and tumor mutation burden (TME) scores were evaluated to identify potentially valid immunotherapy. Finally, chemotherapeutic susceptibility was predicted according to the risk scores and the expression level of the individual prognostic gene.

Results

Construction of a prognostic gene signature in the TCGA cohort

The TCGA-LIHC dataset contains 374 HCC patients, and the ICGC-LIRI-JP dataset contains 260 HCC patients, the clinical characteristics of these patients are displayed in Table S3. As illustrated in Fig .1a, b, 2107 DEGs were identified from the TCGA cohort, among which 55 genes were OSRGs (Fig. 1c). 13 OSRGs were then verified significantly related to shorter OS (Fig. 1d). After LASSO Cox regression analysis, an eight-gene prognostic signature was constructed (Fig .1e, f). To calculate the risk score of each patients, following formula is used: risk score = 0.069*expression level of *G6PD* + 0.177*expression level of *MT3* + 0.206*expression level of *CBX2* + 0.063* expression level of *CDKN2B* + 0.078*expression

level of *CCNA2* + 0.164*expression level of *MAPT* + 0.248*expression level of *EZH2* + 0.213*expression level of *SLC7A11* (Fig. S1). The above eight genes' expression was upregulated in HCC tissue than in normal liver tissue in the TCGA cohort (Fig. S2). We further validated the expression pattern of the proteins encoded by the above genes using clinical specimens in HPA database. All proteins except SLC7A11 were found to be elevated in HCC tissues. No conclusion could be drawn about SLC7A11 due to lack of data. G6PD, MT3, and MAPT were exclusively located in the cytoplasm, CDKN2B was located in both the cytoplasm and nucleus, while CBX2, CCNA2, and EZH2 were located in the nucleus (Fig. 1g).

Validation of the prognostic gene signature

Then we classified the patients into the high-risk score and low-risk score subgroups according to the median cut-off value in the TCGA and ICGC cohorts (Fig.2a). Compared with the low-risk group, patients in the high-risk group had a higher mortality rate (Fig. 2c). In line with this, the K-M curve revealed a significantly shorter OS in the high-risk group (Fig. 2e). The expression heatmap of the eight genes is displayed in Fig. 2g. Time-dependent ROC curves assessed the predictive accuracy of the prognostic gene signature. The area under the ROC curve (AUC) of one, two, and three-year was 0.79, 0.75, and 0.73, respectively, which confirmed the effectiveness of this prognostic model (Fig. 2i). Then, we verified the robustness of the prognostic gene signature using the independent ICGC cohort. The results of patient distribution, K-M curve analysis, and AUC analysis were in line with those of TCGA cohort, further supporting the robustness of the prognostic gene signature (Fig. 2b, d, f, h, j).

Evaluation of the independent prognostic value of risk score and nomogram establishment

We brought the clinicopathological characteristics and risk scores into univariate and multivariate Cox regression analyses to identify the independent prognostic predictors. Univariate Cox analysis of TCGA cohort revealed that stage, T, M, and risk score were significantly correlated with OS (Fig. 3a). In the ICGC cohort, univariate Cox analysis suggested that female gender, stage, and risk score were strongly associated with OS (Fig. 3c). After multivariate Cox analysis, risk score emerged as the only independent factor for efficiently predicting prognosis in both cohorts (Fig. 3b, d). We then constructed nomograms combining clinical variables and risk scores to calculate the total score of each patient with HCC, which could predict the one, two, and three-year OS (Fig. 3e, f). The calibration curves showed the excellent predictive accuracy of the nomograms (Fig. 3g, h).

Immune infiltration and ICI therapy prediction

Next, we employed CIBERSORT algorithm to assess the infiltration of the immune cells of each HCC sample (Fig. S3). As illustrated in Fig. 4a, the memory B cells, activated memory CD4+T cells, follicular helper T cells, and M0 macrophages were more abundant in the high-risk group compared to the low-risk

group. However, naïve B cells, CD8+T cells, resting memory CD4+ T cells, monocytes and eosinophils were reduced in the low-risk group. In addition, there was a positive correlation between the immune checkpoints expression level and risk scores (Fig. 4b). TIDE analysis revealed that the risk scores and TIDE scores were negatively correlated (Fig. 4c). Consistently, the response rate to ICI therapy was expected to be higher in patients suffering from HCC with high risk scores (62% vs. 37%) (Fig. 4d).

Associations of TMB with Risk Score in HCC patients

Next, we investigated the associations of TMB with the risk score. As mentioned before, we stratified HCC patients into high- or low-risk groups in the TCGA cohort. The comprehensive mutation data for each group was represented using a waterfall plot (Fig. 5a). The five most frequently mutated genes were *TP53*(44%), *CTNNB1*(24%), *TTN*(23%), *MUC16*(18%), and *APOB*(11%) in the high-risk group, while *CTNNB1*(27%), *TTN*(23%), *ALB*(13%), *TP53*(12%), and *MUC16*(11%) were the top five in the low-risk group. In addition, the overall genome mutation occurrence rate was 86.71% and 82.49% in the high- and low-risk group, respectively. As displayed in Fig. 5b, the TMB scores were positively correlated with the risk scores. The K-M curve analysis revealed that the patients in the high-TMB group have shorter OS than the patients in the low-TMB group. (Fig. 5c).

Analysis of the Correlation Between Risk Score and Chemotherapy Sensitivity

First, we estimated the chemotherapeutic response using the drug activity and transcriptomic data in the CGP cell lines. In the high-risk group, HCC patients were sensitive to 45 chemotherapy and targeted therapy drugs and were resistant to other 44 drugs, as indicated by the variation of the IC50 (Fig .6a, b). For each prognostic gene in the gene signature, the corresponding expression level was analyzed in the transcriptomic data of NCI-60 cell lines. The top two FDA-approved drugs with the strongest positive or negative association with each gene are shown in Fig. 7. The elevated expression of *G6PD, MT3, CBX2, CDKN2B, CCNA2, MAPT*, and *EZH2* was associated with increased resistance to mitomycin, teniposide, 6-thioguanine, and fulvestrant, etc. By contrast, elevated *CBX2* and *SLC7A11* expression are hallmarks of increased sensitivity to dasatinib, ixazomib citrate, and arsenic trioxide.

Discussion

In the era of precision oncology, the conventionally used serum alpha-fetoprotein test, BCLC staging system, and AJCC staging system do not comply with the prognostic and therapeutic prediction for HCC precise therapy. Some novel diagnostic approaches, including liquid biopsy [11], GALAD model [12], have shown excellent performance in diagnosis and prognosis prediction of HCC. However, major challenges still exist in the bench-to-bedside translation of these technologies.

Here, for the first time, we developed a novel oxidative stress response gene signature to predict the prognosis and therapeutic effect of HCC patients. We first identified DEGs between HCC tissues and normal liver tissues in the TCGA cohort. Then, the 55 shared genes of OSRGs and DEGs were analyzed using univariate Cox regression, which revealed that 13 of these genes were related to OS. A gene signature of eight prognostic genes was then established using the LASSO Cox regression analysis. The prognostic gene signature achieved excellent performance in predicting the OS rate in the TCGA and ICGC cohorts. In addition, the nomograms constructed with risk scores and clinicopathologic factors showed good predictive ability for OS. The multivariate Cox analysis identified the risk score as an independent predictor for prognosis.

The gene signature established in the present study contains eight OSRGs (*G6PD, MT3, CBX2, CDKN2B, CCNA2, MAPT, EZH2, SLC7A11*). Compared with normal tissue, these genes are highly expressed in HCC tissue and are associated with unfavorable prognoses. *G6PD* encodes the protein glucose-6-phosphate dehydrogenase, which can resist damage by oxidative stress in cells [13]. Abnormal activation of G6PD contributes to the progression of many cancers [14]. *MT3* encodes the protein metallothionein3, which displays a solid ROS-scavenging capacity in oxidative stress-conditioned cells[15]. However, the exact role of MT3 in cancer cells remains controversial[16, 17]. As an oncogenic gene [18, 19], *CBX2* is strongly associated with genome-scale DNA methylation in various types of cancer cells, which is a response to micro-environmental stresses, particularly oxidative stress [20]. Recently, H-A Lee et al. reported that oxidative stress enhances *CDKN2B* expression and causes cell cycle arrest in HCC cells [21]. Nonetheless, the correlation between *CDKN2B* expression levels and prognosis is still unclear [22, 23]. *CCNA2* encodes Cyclin A2, which is a suppressor of intracellular oxidative stress [24] that is upregulated in colorectal and breast cancer tissues and is associated with poor prognosis [25, 26]. The *MAPT* encodes the protein Taus, which plays a significant role in the antioxidative response in neurons [27]. Elevated tau has been associated with a poor prognosis in prostate cancer [28]. *EZH2* is an oncogene that is upregulated under oxidative stress induced by H_2O_2 [29, 30]. Finally, SLC7A11 encodes a cystine/glutamate transporter that has been reported to suppress the expression of P-glycoprotein in breast cancer cells induced by ROS [31]. In addition, SLC7A11 was overexpressed in numerous cancers and is correlated with poor survival [32].

We observed that the prognostic gene signature was closely associated with infiltrating immune cells in the tumor microenvironment as memory B cells, activated memory CD4+T cells, follicular helper T cells, and M0 Macrophages were abundant in patients with high risk scores. At present, the interaction between immune checkpoints and oxidative stress has barely been studied. Tang et al. found that treatment with a cocktail of immune checkpoint antibodies increased oxidative stress and T cell infiltration in lung adenocarcinoma [33]. Our data identified various immune checkpoints that have a positive correlation with risk scores, among which PD1, PD-L1, and CTLA4 are common targets for ICI therapy in clinical application. Pre-clinical studies showed that IDO1, TIGIT, LAG3, and TIM-3 are promising therapeutic targets [34]. Although patients with high expression levels of immune checkpoints tend to experience immune evasion and the consequent poor prognosis, the elevated expression of PD1, PD-L1, TIM-3, and

IDO1 may result in a higher response rate to ICI therapy [35-37]. The results of TIDE analysis further supported these findings because patients with HCC having high risk scores were also associated with low TIDE scores, thereby indicating their high response rates to ICI treatment. Previous studies have reported that high TMB indicates a better response to immunotherapy, which could be explained by the fact that mutant proteins encoded by mutated genes in cancer cells make tumors more immunogenic [38, 39]. This study found that the total gene mutation rate was higher in the high-risk group, and that patients with high TMB scores had lower OS rates. Interestingly, the *TP53* mutation rate in the high-risk group is much higher than in the low-risk group (44% vs. 27%). Some research findings suggested that the mutant p53 protein usually loses antioxidant function and increases intracellular ROS, which drives the function switch from a cancer suppressor protein to a cancer promoter protein [40]. Hence, this finding supports our OSRGs-based prognostic gene signature.

In general, HCC cells are resistant to intravenous cytotoxic chemotherapy. Instead, transarterial chemoembolization and oral administration of sorafenib/lenvatinib are the globally-accepted standards for treating advanced HCC. Doxorubicin and cisplatin are the frequently-used drugs in transarterial chemoembolization [41]. In the present study, the patients with HCC in the high-risk group exhibited elevated sensitivity to doxorubicin, afatinib, etoposide, and gemcitabine. Inversely, they were more likely to acquire resistance against sorafenib, the most extensively used multi-targeted tyrosine kinases inhibitor for treating late-stage HCC [42]. Using the NCI-60 data, we verified that each member of the gene signature could potentially indicate susceptibility to several FDA-approved chemotherapeutic drugs. Sensitivity towards some of these drugs has already been proved [26, 43-48]. For most of the prognostic genes, elevated expression levels are associated with increased drug resistance, making them potential targets to overcome this crisis. For example, cisplatin treatment induces ROS production in ovarian cancer, and ROS promotes *EZH2* expression, which inactivates AKT/ERK pathways that confers cisplatin resistance [49].

Conclusion

We established a novel prognostic gene signature consisting of eight oxidative stress response genes, which showed good performance in predicting the prognosis of HCC patients. Our gene signature could also be utilized as a molecular tool for predicting the immunotherapy response and chemotherapy sensitivity which are a requisite for developing precision cancer medicine strategies. To sum up, our study laid the foundation for further search on the oxidative stress response genes and their effect on the prognostic evaluation and therapeutic choice for HCC.

Methods

Databases

We downloaded the transcriptomic and clinical data of HCC from the Liver Hepatocellular Carcinoma (TCGA-LIHC) collected dataset in the TCGA database and the LIRI-JP cohort in the ICGC database. Both

TCGA and ICGC databases are publicly available; hence the ethical review is not required for their use. Oxidative stress response genes were retrieved from the MSigDB database v7.4 (https://www.gsea-msigdb.org/gsea/msigdb/) (Table S1). The expression intensity and distribution of specific proteins in HCC and normal liver tissue were evaluated using clinical specimens from the Human Protein Atlas (HPA) database (https://www.proteinatlas.org/).

Construction and validation of the prognostic oxidative stress response genes signature

We identified the differentially expressed genes (DEGs) between the normal and HCC tissues in TCGA cohort using the "limma" package in R software Version4.0.2 with the following threshold values: $|\log_2 FC| \geq 1$ and adj.p < 0.05. The shared candidate genes of DEGs and OSRGs were analyzed using univariate Cox regression analysis, genes with adj.p < 0.001 were preserved. Then LASSO Cox regression analysis was adopted to construct a prognostic gene signature, implemented using R software with "glmnet" package. The risk score of each patient was determined as follows: Risk score=$\sum$(Coef(i) *Expression of gene(i)). The Kaplan–Meier (K-M) curve was plotted dependent using the "survminer" and "survival" packages in R software. We delineated the receiver operating characteristic (ROC) curves with the "timeROC" package in R software to assess the accuracy of the prognostic gene signature.

Nomogram establishment

A forecast nomogram was developed by incorporating risk scores, age, gender, stage, and TNM classification with the R package "RMS." The one, two, three-year OS probabilities were estimated using the total points. Calibration curves were used to evaluate the accuracy.

Assessment of immune cell infiltration

We used the CIBERSORT algorithm to quantify the subsets of infiltrating immune cells in the tumor environment of HCC samples. CIBERSORT is a deconvolution method based on bulk gene expression to estimate specific immune cell types [50].

Prediction of immune checkpoint inhibition (ICI) therapy

The tumor immune dysfunction exclusion (TIDE) analysis platform was utilized to predict the responses to ICI therapy (http://tide.dfci.harvard.edu/). TIDE is a computational method that uses specific gene markers to predict the response to ICI therapy [51]. A high TIDE score represents a low response rate to ICI.

Calculation of TMB scores

TMB is a measure of the gene mutations frequency in a cancer cell. We obtained the VarScan processed somatic mutation data of HCC from TCGA database. Strawberry-Perl version5.30.1 based on the JAVA8 platform was used to determine the TMB score depending on the genome mutation information of each HCC sample.

Chemotherapy response estimation

To estimate the association between drug therapeutic response and risk scores, the R package “pRRophetic” was adopted to generate each drug's half-maximal inhibitory concentration (IC50 value) for HCC patients. The pRRophetic package was constructed based on the chemical screening data from the Cancer Genome Project (CGP) dataset [52]. To explore the drug response prediction from the individual prognostic gene, we analyzed the pharmacological activity data of 218 FDA-approved drugs (Table S2) from the NCI-60 cancer cell lines, which were downloaded from the CellMiner database Version2021.2 (https://discover.nci.nih.gov/cellminer).

Statistical analysis

DEGs among HCC and normal liver tissues were compared using Wilcoxon signed-rank test. The K-M curve and the log-rank test were used to assess the difference in OS between groups. The correlation analysis was performed using the Pearson correlation coefficient. GraphPad Prism Version7.0.4 and R software Version 4.0.2 were utilized to make diagrams. P-value <0.05 was considered statistically significant.

Abbreviations

TCGA: The Cancer Genome Atlas; ICGC: International Cancer Genome Consortium; OSRGs: Oxidative stress response genes; ICI: immune checkpoint inhibition; HCC: Hepatocellular carcinoma; ROS: reactive oxygen species; OS: overall survival; TME: tumor mutation burden; AUC: area under the ROC curve; ROC: receiver operating characteristic; TIDE: tumor immune dysfunction exclusion; DEGs: differentially expressed genes; HPA: Human Protein Atlas; CGP: Cancer Genome Project; Kaplan–Meier curve: K-M curve.

Declarations

Ethics approval and consent to participate

Not applicable.

Consent for publication

Not applicable.

Availability of data and materials

The public datasets analyzed in this study can be downloaded here: https://portal.gdc.cancer.gov/repository and https://dcc.icgc.org/releases/current/Projects/LIRI-JP. All codes used in this study are available from the corresponding author upon reasonable request.

Competing interests

The authors declare no competing interests.

Funding

No funding was received.

Author contribution

Junjie Hong: Data analysis, Original draft preparation; Xiujun Cai: Conceptualization and Investigation, Manuscript review and editing. All authors reviewed the manuscript.

Acknowledgements

We thank Editage for the English language editing.

References

1. Asafo-Agyei KO, Samant H. Hepatocellular Carcinoma. 2021. StatPearls Publishing. Treasure Island (FL).
2. Chen M, Xie S Therapeutic targeting of cellular stress responses in cancer. Thoracic cancer. 2018;9(12):1575-82.
3. Wang Z, Li Z, Ye Y, Xie L, Li W Oxidative Stress and Liver Cancer: Etiology and Therapeutic Targets. Oxid. Med. Cell. Longev. 2016;2016:7891574.
4. Hayes JD, Dinkova-Kostova AT, Tew KD Oxidative Stress in Cancer. Cancer Cell. 2020;38(2):167-97.
5. Kim J, Kim J, Bae J-S ROS homeostasis and metabolism: a critical liaison for cancer therapy. Exp. Mol. Med. 2016;48(11):e269-e.

6. Nogueira V, Hay N Molecular pathways: reactive oxygen species homeostasis in cancer cells and implications for cancer therapy. Clin. Cancer Res. 2013;19(16):4309-14.
7. Tafani M, Sansone L, Limana F, Arcangeli T, De Santis E, Polese M, et al. The Interplay of Reactive Oxygen Species, Hypoxia, Inflammation, and Sirtuins in Cancer Initiation and Progression. Oxid. Med. Cell. Longev. 2016;2016:3907147.
8. Chio IIC, Tuveson DA ROS in Cancer: The Burning Question. Trends Mol. Med. 2017;23(5):411-29.
9. Yang H, Villani RM, Wang H, Simpson MJ, Roberts MS, Tang M, et al. The role of cellular reactive oxygen species in cancer chemotherapy. J. Exp. Clin. Cancer Res. 2018;37(1):266.
10. Dalleau S, Baradat M, Guéraud F, Huc L Cell death and diseases related to oxidative stress:4-hydroxynonenal (HNE) in the balance. Cell Death Differ. 2013;20(12):1615-30.
11. von Felden J, Garcia-Lezana T, Schulze K, Losic B, Villanueva A Liquid biopsy in the clinical management of hepatocellular carcinoma. Gut. 2020;69(11):2025-34.
12. Johnson PJ, Pirrie SJ, Cox TF, Berhane S, Teng M, Palmer D, et al. The detection of hepatocellular carcinoma using a prospectively developed and validated model based on serological biomarkers. Cancer Epidemiol. Biomarkers Prev. 2014;23(1):144-53.
13. Nóbrega-Pereira S, Fernandez-Marcos PJ, Brioche T, Gomez-Cabrera MC, Salvador-Pascual A, Flores JM, et al. G6PD protects from oxidative damage and improves healthspan in mice. Nature Communications. 2016;7(1):10894.
14. Yang H-C, Wu Y-H, Yen W-C, Liu H-Y, Hwang T-L, Stern A, et al. The redox role of G6PD in cell growth, cell death, and cancer. Cells. 2019;8(9):1055.
15. Uchida Y, Gomi F, Masumizu T, Miura Y Growth inhibitory factor prevents neurite extension and the death of cortical neurons caused by high oxygen exposure through hydroxyl radical scavenging. J. Biol. Chem. 2002;277(35):32353-9.
16. Kmiecik AM, Pula B, Suchanski J, Olbromski M, Gomulkiewicz A, Owczarek T, et al. Metallothionein-3 increases triple-negative breast cancer cell invasiveness via induction of metalloproteinase expression. PLoS One. 2015;10(5):e0124865.
17. Tao Y-F, Xu L-X, Lu J, Cao L, Li Z-H, Hu S-Y, et al. Metallothionein III (MT3) is a putative tumor suppressor gene that is frequently inactivated in pediatric acute myeloid leukemia by promoter hypermethylation. J. Transl. Med. 2014;12(1):1-14.
18. Zhou H, Xiong Y, Liu Z, Hou S, Zhou T Expression and prognostic significance of CBX2 in colorectal cancer: database mining for CBX family members in malignancies and vitro analyses. Cancer Cell Int. 2021;21(1):402.
19. Zheng S, Lv P, Su J, Miao K, Xu H, Li M Overexpression of CBX2 in breast cancer promotes tumor progression through the PI3K/AKT signaling pathway. American journal of translational research. 2019;11(3):1668-82.
20. Cao S, Zhou Y, Wu Y, Song T, Alsaihati B, Xu Y Transcription regulation by DNA methylation under stressful conditions in human cancer. Quantitative Biology. 2017;5(4):328-37.

21. Lee H-A, Chu K-B, Moon E-K, Quan F-S Histone Deacetylase Inhibitor-Induced CDKN2B and CDKN2D Contribute to G2/M Cell Cycle Arrest Incurred by Oxidative Stress in Hepatocellular Carcinoma Cells via Forkhead Box M1 Suppression. J. Cancer. 2021;12(17):5086.
22. Genescà E, Lazarenkov A, Morgades M, Berbis G, Ruiz-Xivillé N, Gómez-Marzo P, et al. Frequency and clinical impact of CDKN2A/ARF/CDKN2B gene deletions as assessed by in-depth genetic analyses in adult T cell acute lymphoblastic leukemia. J. Hematol. Oncol. 2018;11(1):1-4.
23. Tu Q, Hao J, Zhou X, Yan L, Dai H, Sun B, et al. CDKN2B deletion is essential for pancreatic cancer development instead of unmeaningful co-deletion due to juxtaposition to CDKN2A. Oncogene. 2018;37(1):128-38.
24. Xu S, Wu W, Huang H, Huang R, Xie L, Su A, et al. The p53/miRNAs/Ccna2 pathway serves as a novel regulator of cellular senescence: Complement of the canonical p53/p21 pathway. Aging Cell. 2019;18(3):e12918.
25. Gan Y, Li Y, Li T, Shu G, Yin G CCNA2 acts as a novel biomarker in regulating the growth and apoptosis of colorectal cancer. Cancer Manag. Res. 2018;10:5113.
26. Gao T, Han Y, Yu L, Ao S, Li Z, Ji J CCNA2 is a prognostic biomarker for ER+ breast cancer and tamoxifen resistance. PLoS One. 2014;9(3):e91771.
27. Wang X, Campbell MR, Lacher SE, Cho H-Y, Wan M, Crowl CL, et al. A polymorphic antioxidant response element links NRF2/sMAF binding to enhanced MAPT expression and reduced risk of Parkinsonian disorders. Cell reports. 2016;15(4):830-42.
28. Schroeder C, Grell J, Hube-Magg C, Kluth M, Lang D, Simon R, et al. Aberrant expression of the microtubule-associated protein tau is an independent prognostic feature in prostate cancer. BMC Cancer. 2019;19(1):1-10.
29. Zheng X, Tsou P-S, Sawalha AH Increased Expression of EZH2 Is Mediated by Higher Glycolysis and mTORC1 Activation in Lupus CD4+ T Cells. Immunometabolism. 2020;2(2).
30. Duan R, Du W, Guo W EZH2: a novel target for cancer treatment. J. Hematol. Oncol. 2020;13:1-12.
31. Ge C, Cao B, Feng D, Zhou F, Zhang J, Yang N, et al. The down-regulation of SLC7A11 enhances ROS induced P-gp over-expression and drug resistance in MCF-7 breast cancer cells. Sci. Rep. 2017;7(1):1-11.
32. Lin W, Wang C, Liu G, Bi C, Wang X, Zhou Q, et al. SLC7A11/xCT in cancer: biological functions and therapeutic implications. Am. J. Cancer Res. 2020;10(10):3106.
33. Tang J, Ramis-Cabrer D, Wang X, Barreiro E Immunotherapy with Monoclonal Antibodies in Lung Cancer of Mice: Oxidative Stress and Other Biological Events. Cancers (Basel). 2019;11(9):1301.
34. Qin S, Xu L, Yi M, Yu S, Wu K, Luo S Novel immune checkpoint targets: moving beyond PD-1 and CTLA-4. Mol. Cancer. 2019;18(1):1-14.
35. Buchbinder EI, Desai A CTLA-4 and PD-1 Pathways: Similarities, Differences, and Implications of Their Inhibition. Am. J. Clin. Oncol. 2016;39(1).

36. Kato R, Jinnouchi N, Tuyukubo T, Ikarashi D, Matsuura T, Maekawa S, et al. TIM3 expression on tumor cells predicts response to anti-PD-1 therapy for renal cancer. Transl. Oncol. 2021;14(1):100918.
37. Seeber A, Klinglmair G, Fritz J, Steinkohl F, Zimmer KC, Aigner F, et al. High IDO-1 expression in tumor endothelial cells is associated with response to immunotherapy in metastatic renal cell carcinoma. Cancer Sci. 2018;109(5):1583-91.
38. Cao D, Xu H, Xu X, Guo T, Ge W High tumor mutation burden predicts better efficacy of immunotherapy: a pooled analysis of 103078 cancer patients. Oncoimmunology. 2019;8(9):e1629258.
39. Goodman AM, Kato S, Bazhenova L, Patel SP, Frampton GM, Miller V, et al. Tumor mutational burden as an independent predictor of response to immunotherapy in diverse cancers. Mol. Cancer Ther. 2017;16(11):2598-608.
40. Cordani M, Butera G, Pacchiana R, Masetto F, Mullappilly N, Riganti C, et al. Mutant p53-Associated Molecular Mechanisms of ROS Regulation in Cancer Cells. Biomolecules. 2020;10(3).
41. Lencioni R, Petruzzi P, Crocetti L Chemoembolization of hepatocellular carcinoma. Seminars in interventional radiology. 2013;30(1):3-11.
42. Marisi G, Cucchetti A, Ulivi P, Canale M, Cabibbo G, Solaini L, et al. Ten years of sorafenib in hepatocellular carcinoma: Are there any predictive and/or prognostic markers? World J. Gastroenterol. 2018;24(36):4152-63.
43. Robert SM, Buckingham SC, Campbell SL, Robel S, Holt KT, Ogunrinu-Babarinde T, et al. SLC7A11 expression is associated with seizures and predicts poor survival in patients with malignant glioma. Sci. Transl. Med. 2015;7(289):289ra86-ra86.
44. Yamawaki K, Mori Y, Sakai H, Kanda Y, Shiokawa D, Ueda H, et al. Integrative analyses of gene expression and chemosensitivity of patient-derived ovarian cancer spheroids link G6PD-driven redox metabolism to cisplatin chemoresistance. Cancer Lett. 2021;521:29-38.
45. Wheeler LJ, Watson ZL, Qamar L, Yamamoto TM, Post MD, Berning AA, et al. CBX2 identified as driver of anoikis escape and dissemination in high grade serous ovarian cancer. Oncogenesis. 2018;7(11):92.
46. Rodrigo MAM, Michalkova H, Strmiska V, Casar B, Crespo P, de los Rios V, et al. Metallothionein-3 promotes cisplatin chemoresistance remodelling in neuroblastoma. Sci. Rep. 2021;11(1):5496.
47. Yang J, Yu Y, Liu W, Li Z, Wei Z, Jiang R Microtubule-associated protein tau is associated with the resistance to docetaxel in prostate cancer cell lines. Research and reports in urology. 2017;9:71.
48. Zhang T, Ma K, Huang J, Wang S, Liu Y, Fan G, et al. CDKN2B is critical for verapamil-mediated reversal of doxorubicin resistance in hepatocellular carcinoma. Oncotarget. 2017;8(66):110052-63.
49. Sun J, Cai X, Yung MM, Zhou W, Li J, Zhang Y, et al. miR-137 mediates the functional link between c-Myc and EZH2 that regulates cisplatin resistance in ovarian cancer. Oncogene. 2019;38(4):564-80.
50. Chen B, Khodadoust MS, Liu CL, Newman AM, Alizadeh AA Profiling Tumor Infiltrating Immune Cells with CIBERSORT. Methods in molecular biology (Clifton, N.J.). 2018;1711:243-59.

51. Jiang P, Gu S, Pan D, Fu J, Sahu A, Hu X, et al. Signatures of T cell dysfunction and exclusion predict cancer immunotherapy response. Nat. Med. 2018;24(10):1550-8.

52. Geeleher P, Cox N, Huang RS pRRophetic: an R package for prediction of clinical chemotherapeutic response from tumor gene expression levels. PLoS One. 2014;9(9):e107468.

Figures

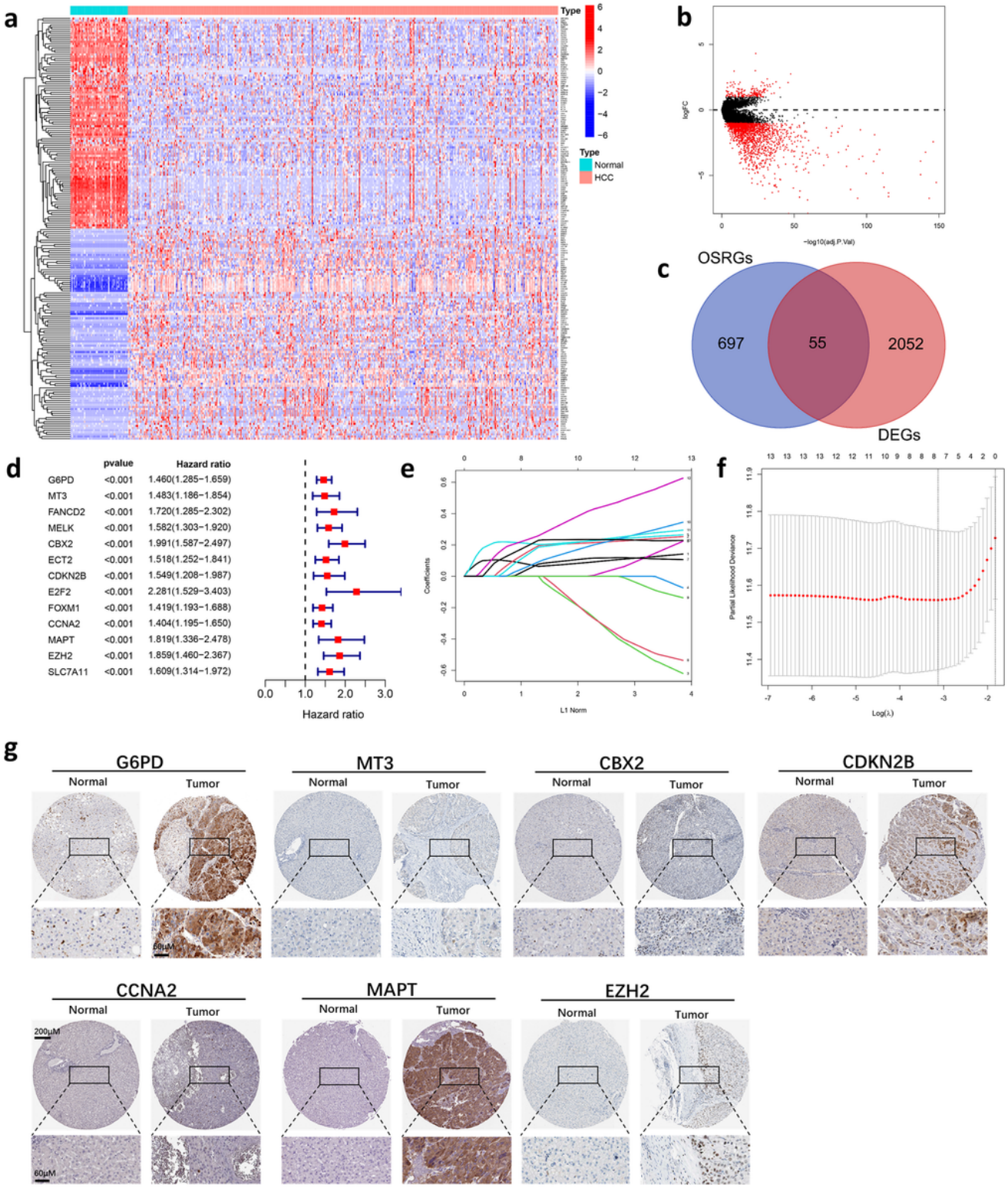

Figure 1

Construction of oxidative stress response genes (OSRGs) signature. (a,b) Heatmap and volcano plot of the differentially expressed genes (DEGs) in normal and HCC tissues. (c) Venn diagram of the shared genes of DEGs and OSRGs. (d) Screening of the candidate OSRGs using univariate Cox regression analysis. (e,f) The LASSO Cox regression yieled a prognostic gene signature. Ten fold cross-validation was used for the parameter chosen. (g) Representative immunohistochemistry images of G6PD, MT3, CVX2, CDKN2B, CCNA2, MAPT, EZH2 in normal and HCC tissues.

Figure 2

Prognostic performance of the gene signature. (a, c, e, g, i) TCGA cohort, (b, d, f, h, j) ICGC cohort. (a, c) The distribution of patients with high- or low-risk scores. (b, d) The survival status of each patient. (e, f) Kaplan-Meier curve shows the different overall survival between the high- and low-risk groups. (g, h) Heatmap shows the expression level of each gene in the gene signature. (i, j) 1,2,3-year ROC curves and AUC for overall survival.

Figure 3

Identify the independent risk factors for OS and establishment of nomograms. (a, b, e, g) TCGA cohort, (c, d, f, h) ICGC cohort. (a, c) Identify the OS-related risk factors using univariate Cox regression analysis. (b, d) Multivariate Cox regression for assessing the independent risk factor for OS. (E, F) Construction of nomograms with the risk scores and clinicopathological parameters. (G, H) Calibration curves to evaluate the precision of nomograms.

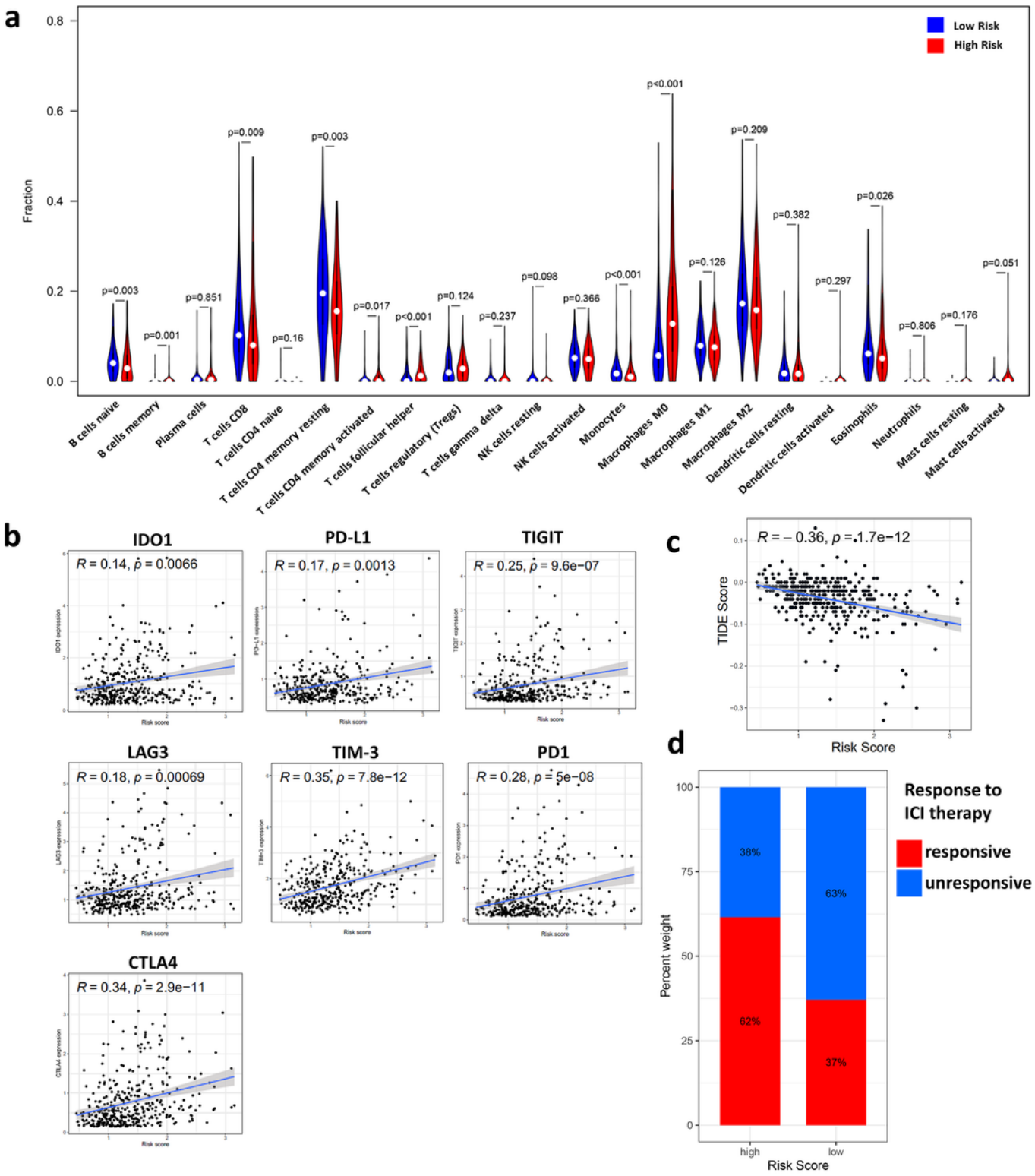

Figure 4

Estimation of the response to ICI therapy. (a) The fraction of infiltrating immune cells in different subgroups. (b) Association between the risk scores and expression level of various immune checkpoints. (c) Risk scores positively correlated to TIDE scores. (d) Responsive rate to ICI therapy in high- and low-risk groups. ICI, immune checkpoints inhibition.

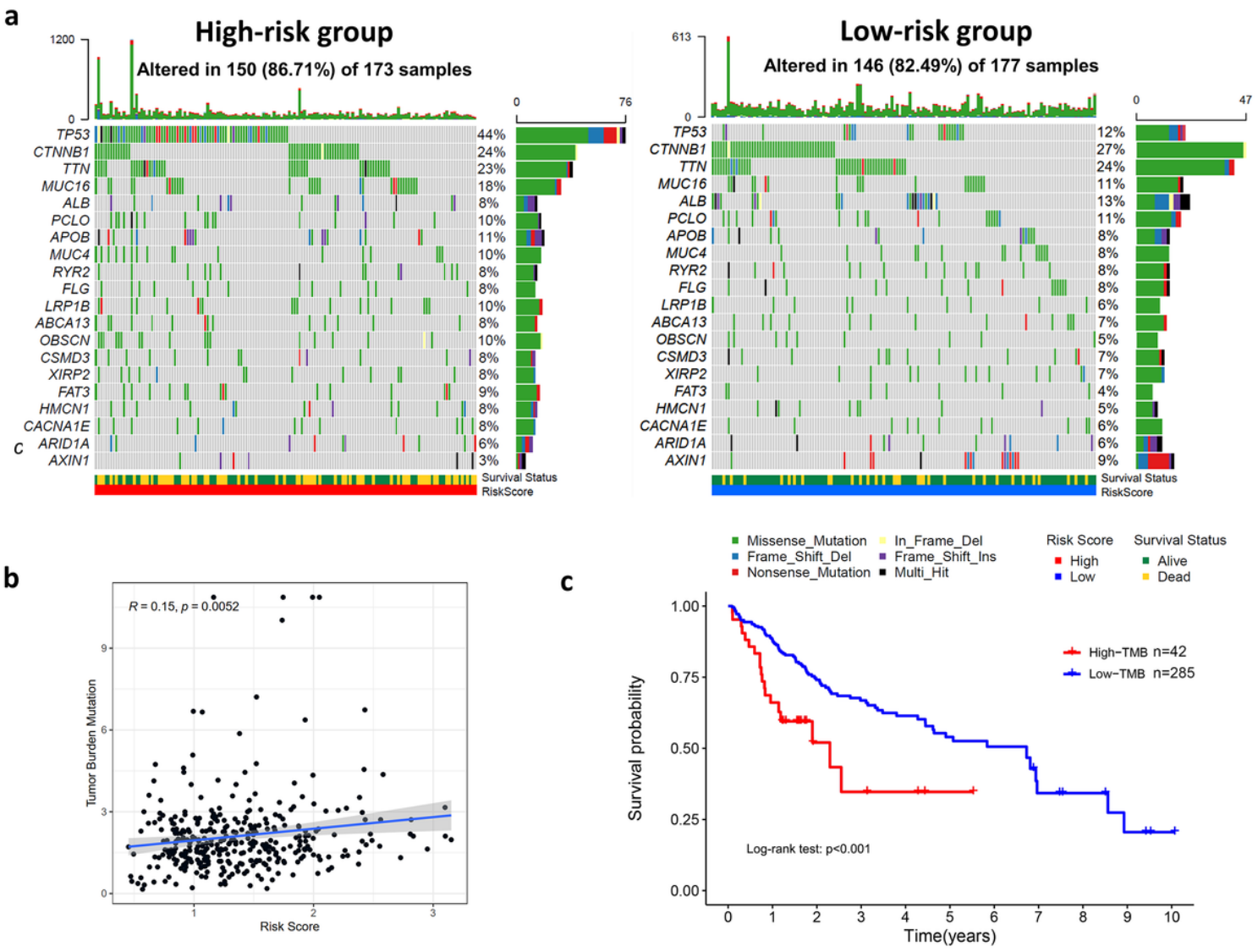

Figure 5

Tumor mutation burden (TMB) map. (a) The top 20 mutated genes in the high-risk and low-risk groups. (b) The correlation between tumor mutation burden scores and risk scores. (c) Kaplan-Meier analysis shows the patients with high TMB scores have worse OS.

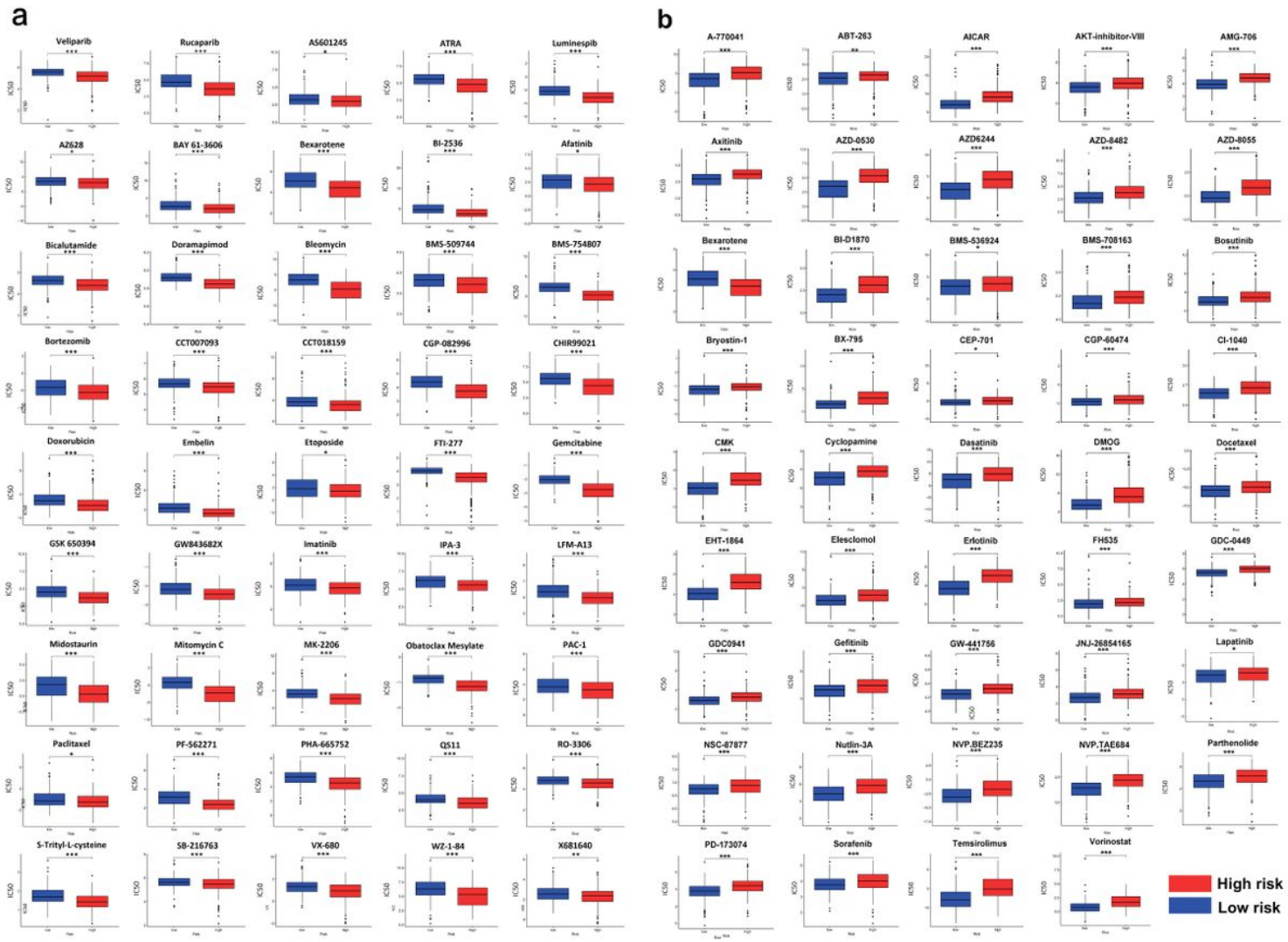

Figure 6

HCC patients with high risk scores were sensitive (a) or resistant (b) to indicated chemotherapy drugs. (*P < 0.05,**P<0.01,***P<0.001)

Figure 7

The correlation between the expression level of each prognostic gene and the drug response.

Supplementary Files

This is a list of supplementary files associated with this preprint. Click to download.

- Supplementalfiguresandtables.docx